Allosteric Modulation Balances Thermodynamic Stability and Restores Function of ΔF508 CFTR

Andrei A. Aleksandrov[1,2]**, Pradeep Kota**[1,3]**, Liying Cui**[1,2]**, Tim Jensen**[1,2]**, Alexey E. Alekseev**[4]**, Santiago Reyes**[4]**, Lihua He**[1,2]**, Martina Gentzsch**[2,5]**, Luba A. Aleksandrov**[1,2]**, Nikolay V. Dokholyan**[1,3] **and John R. Riordan**[1,2]*****

[1]*Department of Biochemistry and Biophysics, The University of North Carolina at Chapel Hill, Chapel Hill, NC 27599, USA*

[2]*Cystic Fibrosis Treatment and Research Center, The University of North Carolina at Chapel Hill, Chapel Hill, NC 27599, USA*

[3]*Molecular and Cellular Biophysics Program, The University of North Carolina at Chapel Hill, Chapel Hill, NC 27599, USA*

[4]*Department of Medicine, Division of Cardiovascular Diseases, Mayo Clinic, 200 First Street Southwest, Rochester, Minnesota 55905, USA*

[5]*Department of Cell and Development Biology, The University of North Carolina at Chapel Hill, Chapel Hill, NC 27599, USA*

Most cystic fibrosis is caused by a deletion of a single residue (F508) in CFTR (cystic fibrosis transmembrane conductance regulator) that disrupts the folding and biosynthetic maturation of the ion channel protein. Progress towards understanding the underlying mechanisms and overcoming the defect remains incomplete. Here, we show that the thermal instability of human ΔF508 CFTR channel activity evident in both cell-attached membrane patches and planar phospholipid bilayers is not observed in corresponding mutant CFTRs of several non-mammalian species. These more stable orthologs are distinguished from their mammalian counterparts by the substitution of proline residues at several key dynamic locations in first N-terminal nucleotide-binding domain (NBD1), including the structurally diverse region, the γ-phosphate switch loop, and the regulatory insertion. Molecular dynamics analyses revealed that addition of the prolines could reduce flexibility at these locations and increase the temperatures of unfolding transitions of ΔF508 NBD1 to that of the wild type. Introduction of these prolines experimentally into full-length human ΔF508 CFTR together with the already recognized I539T suppressor mutation, also in the structurally diverse region, restored channel function and thermodynamic stability as well as its trafficking to and lifetime at the

cell surface. Thus, while cellular manipulations that circumvent its culling by quality control systems leave ΔF508 CFTR dysfunctional at physiological temperature, restoration of the delicate balance between the dynamic protein's inherent stability and channel activity returns a near-normal state.

Introduction

CFTR (cystic fibrosis transmembrane conductance regulator) is a highly dynamic multidomain membrane protein that is folded and assembled slowly and inefficiently with only ~25% of nascent chains achieving a mature stable state.[1] This inefficient maturation is exacerbated by the most common cystic fibrosis mutation, ΔF508; that is, little or no maturation occurs and the polypeptide succumbs to cellular quality control systems and is degraded.[2] It was soon recognized that the mutant protein could mature if it was expressed in cells maintained at temperatures <30 °C.[3] This thermal sensitivity, combined with the finding that some osmolytes promoted maturation of the protein,[4] supported the notion that ΔF508 caused a protein folding defect, as did the observation of increased sensitivity to proteolysis.[5] Initial biophysical studies of the influence of ΔF508 on the chemical denaturation of the isolated N-terminal nucleotide-binding domain (NBD1) suggested that the primary impact might be kinetic rather than thermodynamic.[6] However, more recent dissections of both thermal and chemical unfolding[7,8] have convincingly demonstrated that the mutation causes substantial thermodynamic instability, despite the fact that the overall folds of wild type (WT) and ΔF508 NBD1 are not different.[9] Extensive efforts have been directed at overcoming this cellular phenotype.[10] In addition to the permissive effects of low temperature, small molecules discovered in cell-based screens also have been found to promote traffic to the cell surface.[11,12] However, channel activity of the rescued mutant is detected only below ~30 °C or very transiently at higher temperatures.[13,14]

Thus, it has become apparent that a variety of cellular manipulations can result in ΔF508 CFTR export from the endoplasmic reticulum and traffic to the plasma membrane without the protein having been thermodynamically stabilized. As one approach to gain an understanding of what is required to increase the thermal stability, we have sought to identify differences in CFTR orthologs from other species that might reduce or eliminate the destabilizing impact of ΔF508.[15–18] While other mammalian species that were tested responded similarly to the deletion as the human, some non-mammalian species, most notably avian, not only matured and trafficked to the plasma membrane of mammalian cells but also exhibited robust channel activity at temperatures up to at least 40 °C for prolonged periods. By mimicking some of the NBD1 sequence differences between avian and human CFTR, it was possible to generate a thermally stable human ΔF508 CFTR. Insight into the structural and dynamic bases of these crucial restorative thermodynamic effects was derived from molecular dynamics simulations.

Results

Low temperature plus corrector-rescued ΔF508 CFTR channel remains thermodynamically unstable

We had shown earlier that trafficking-rescued ΔF508 channels remained thermally sensitive in planar lipid bilayers,[19,20] and Wang *et al.* have recently made similar observations in excised membrane patches.[14] To determine whether this thermal instability was exhibited by rescued mutant channels on intact cells, we performed cell-attached patch-clamp experiments. Cell-attached patches of baby hamster kidney (BHK) cells stably expressing either WT or ΔF508 CFTR at 27 °C were analyzed over a range of increasing temperatures (Fig. 1). Single-channel currents were recorded initially at 27 °C prior to a continuous ramp up to 32 °C. WT gating transitions became more frequent as the temperature was increased and remained stable at 32 °C. With the ΔF508-expressing cells that had been grown at 27 °C and treated with two of the more effective small-molecule correctors of its maturation [Corrector-4a (*N*-[2-(5-chloro-2-methoxy-phenyla-mino)-4′-methyl-[4,5′]bithiazolyl-2′-yl]-benzamide) and VRT-325 (4-cyclohexyloxy-2-{1-[4-(4-methoxy-benzensulfonyl)-piperazin-1-yl]-ethyl}-quinazolin)], gating at 27 °C was similar to that of the WT. However, in marked contrast to the WT, when the temperature was increased above 27 °C, gating transitions of the rescued mutant became progressively less frequent and soon nearly disappeared. Thus, in their native plasma membrane environment, rescued ΔF508 CFTR channels rapidly lose activity even before physiological temperature is reached.
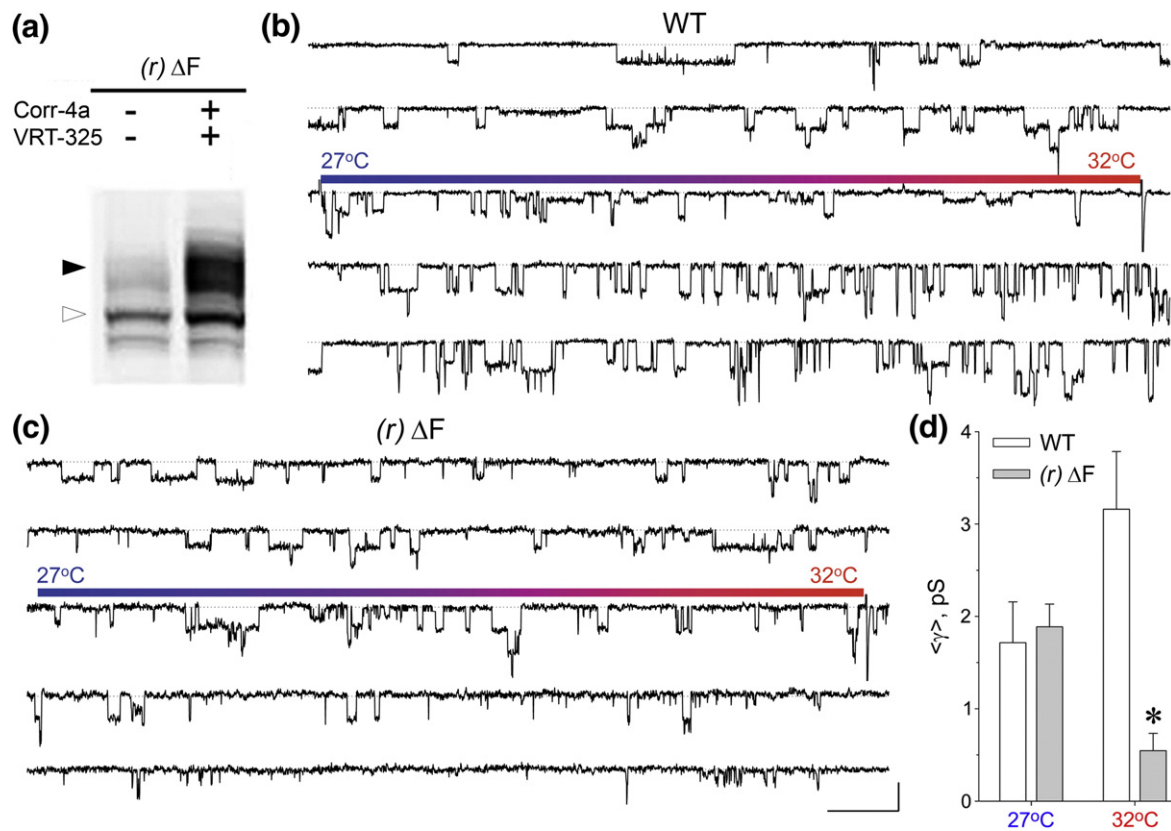
Fig. 1. Corrector plus low temperature-rescued human ΔF508 CFTR in cell-attached patches is thermolabile. (a) Western blot showing formation of a slower migrating diffuse mature band in BHK cells stably expressing ΔF508 CFTR mutant grown at 27 °C [(r)ΔF] without (left lane) or with (right lane) exposure overnight to correctors VRT-325 and Corrector-4a at 10 μM. Positions of immature and mature bands are shown on the left by open and filled arrowheads, respectively. (b) Cell-attached recordings of the WT CFTR ion channels beginning at 27 °C and then, where indicated, ramped up to 32 °C at a rate of 1 °C/10 s. Prior to recording, cells were perfused with a "cation-free" solution containing 150 mM Tris–HCl, pH 7.2, 1 mM EGTA, and 1 g/l glucose supplemented with 15 μM forskolin to activate CFTR ion channel function. The upper level in each trace represents overall closed state for all channels while downward deflections correspond to channel openings and each next lower level represents one more channel opening. (c) Cell-attached recordings of ΔF508 CFTR rescued by low temperature and correctors [(r)ΔF] with the same experimental protocol as in (b). The x-axis scale bar represents 4 s and the y-axis scale bar represents 1 pA for both (b) and (c). (d) Since the gating kinetics of the ΔF508 CFTR is unstable, the bar graph of mean conductance of single structural units ⟨γ⟩ that we consider as a measure of functional capacity for the WT and (r)ΔF at +27 °C and 32 °C is shown instead of probability to be open (P_o). For WT CFTR, ⟨γ⟩ was obtained from continuous 100-s recordings at each temperature and normalized to the number of channels in the patch, while for (r)ΔF, it was calculated from 300 s of recordings at 27 °C and the following 180 s at 32 °C and normalized. In cell-attached configuration, the single-channel chord conductance of both WT and temperature-rescued ΔF508 CFTR was estimated as 8.5 pS at 27 °C and 11.3 pS at 32 °C. The asterisk indicates significant differences from WT CFTR ($p < 0.05$).

Variable influence of the ΔF508 mutation on CFTRs of different species

The ΔF508 mutation is believed to have occurred once in the human population, and it is unknown if it has occurred and what its influence might be in other organisms in which CFTR is functionally important. To investigate this issue, we have expressed CFTR orthologs from several different mammalian and non-mammalian species in human embryonic kidney (HEK)-293 cells. WT but not ΔF508 versions of CFTRs of some of these species have been studied previously.[15–18] These orthologs were expressed, trafficked to the plasma membrane, and exhibited distinctive single-channel properties (Fig. S1). With the ΔF508 versions, Western blotting revealed striking differences in the cellular maturation of the protein, that is, conversion of the more rapidly migrating form with core oligosaccharides to the more slowly migrating form with complex oligosaccharides (Fig. 2a). While the ΔF508 constructs matured at least somewhat at the more permissive 27 °C, there were very clear differences in maturation of the mutants at 37 °C. The sheep
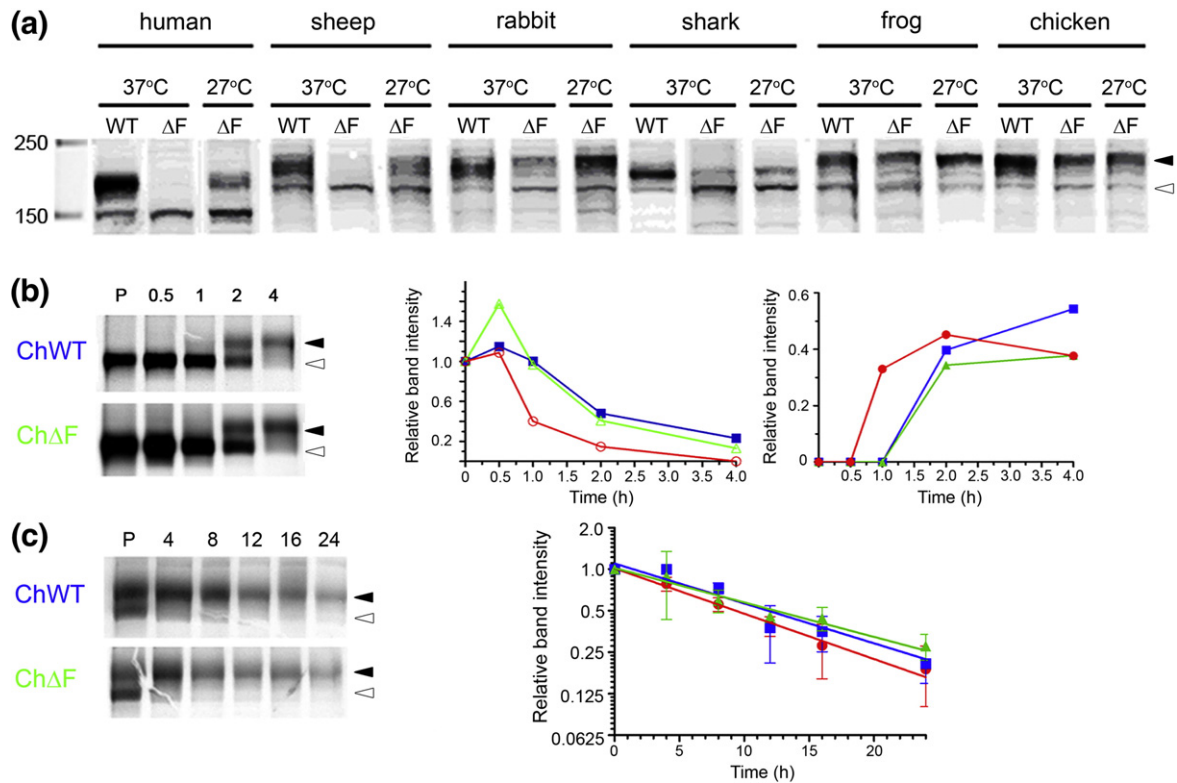
Fig. 2. Maturation and lifetimes of WT and ΔF508 CFTRs from different species. (a) Western blots showing relative amounts of smaller immature and larger mature bands. Cell growth temperatures and genotypes are indicated above the lanes. C-terminal green fluorescent protein tags are present in all species except human, accounting for their slower mobilities. Faster mobility of shark bands is due to glycosylation of one site (rather than two sites); 7.5% acrylamide SDS-PAGE blot probed with mAb 596. (b) Chicken CFTR short-term pulse-chase experiments with ^{35}S-methionine (20 min pulse; chase in hours). Autoradiograms shown were also quantified electronically (Packard Instant Imager), and rates of disappearance of immature precursors and appearance of mature products were graphed. Symbols: human WT, red; chicken WT, blue; chicken ΔF509, green. (c) Long-term pulse-chase experiments showing turnover rates of mature species. Experimental data shown on the graph are mean value ± standard error of the mean from three independent experiments.

ΔF508 CFTR appeared similar to human, maturing somewhat at 27 °C but not at 37 °C. The rabbit mutant protein matured as well as the WT at 27 °C and also detectably at 37 °C. This low-level maturation of rabbit ΔF508 CFTR may reflect primarily the I539T substitution (see below),

Fig. 3. WT and ΔF509 chicken CFTR have similar ATP binding and ion channel activities. (a) Membranes containing human WT (WT), temperature-rescued human ΔF508 [(r)ΔF], chicken WT (ChWT), or chicken ΔF509 (ChΔF) CFTR were incubated with 25 μM [γ^{32}P]-8N$_3$ATP at 4 °C or 35 °C (left panels) and irradiated at 254 nm for 2 min and digested with trypsin (10 μg/ml) for 15 min at 4 °C. Following this limited proteolysis, membranes were solubilized in RIPA buffer, immunoprecipitated with an antibody recognizing an N-terminal epitope (mAb 13-4), subjected to SDS-PAGE (4–20% acrylamide gradient gels), and transferred to nitrocellulose for autoradiographic detection of ^{32}P radioactivity. In the right panels, the labeled membranes were (+) or were not (−) washed free of bulk nucleotide before solubilization. (b) Iodide efflux from BHK-21 cells stably expressing the following: WT human CFTR, red; WT chicken CFTR, blue; ΔF509 chicken CFTR, green; human ΔF508CFTR, purple. After iodide loading, extracellular iodide was removed by rinsing the cells with iodide-free efflux buffer (same as the loading buffer except NaNO$_3$ replaced NaI). Samples were collected by replacing the efflux buffer (1 ml volume) with fresh solution at 1-min intervals. The first four samples were used to establish the baseline. Stimulation cocktail with PKA agonists (10 μM forskolin, 100 μM dibutyl-cAMP, and 1 mM 3-isobuty-1-methylxanthine) was added, and iodide efflux was measured using an iodide-selective electrode. At the end of each assay, efflux buffer containing 0.1% NP-40 was added (shown by arrow) to release any retained iodide. Experimental data are shown as mean values ± standard error of the mean from at least three independent experiments. (c) Single-channel activities also at 25 °C. The upper level in each trace represents closed state, and downward deflections correspond to channel opening. All-point histograms fitted by two-peak Gaussians (red line) are to the left of each tracing and single-channel conductance (γ) and open probabilities (P$_o$) above. The x-axis scale bar represents 10 s.
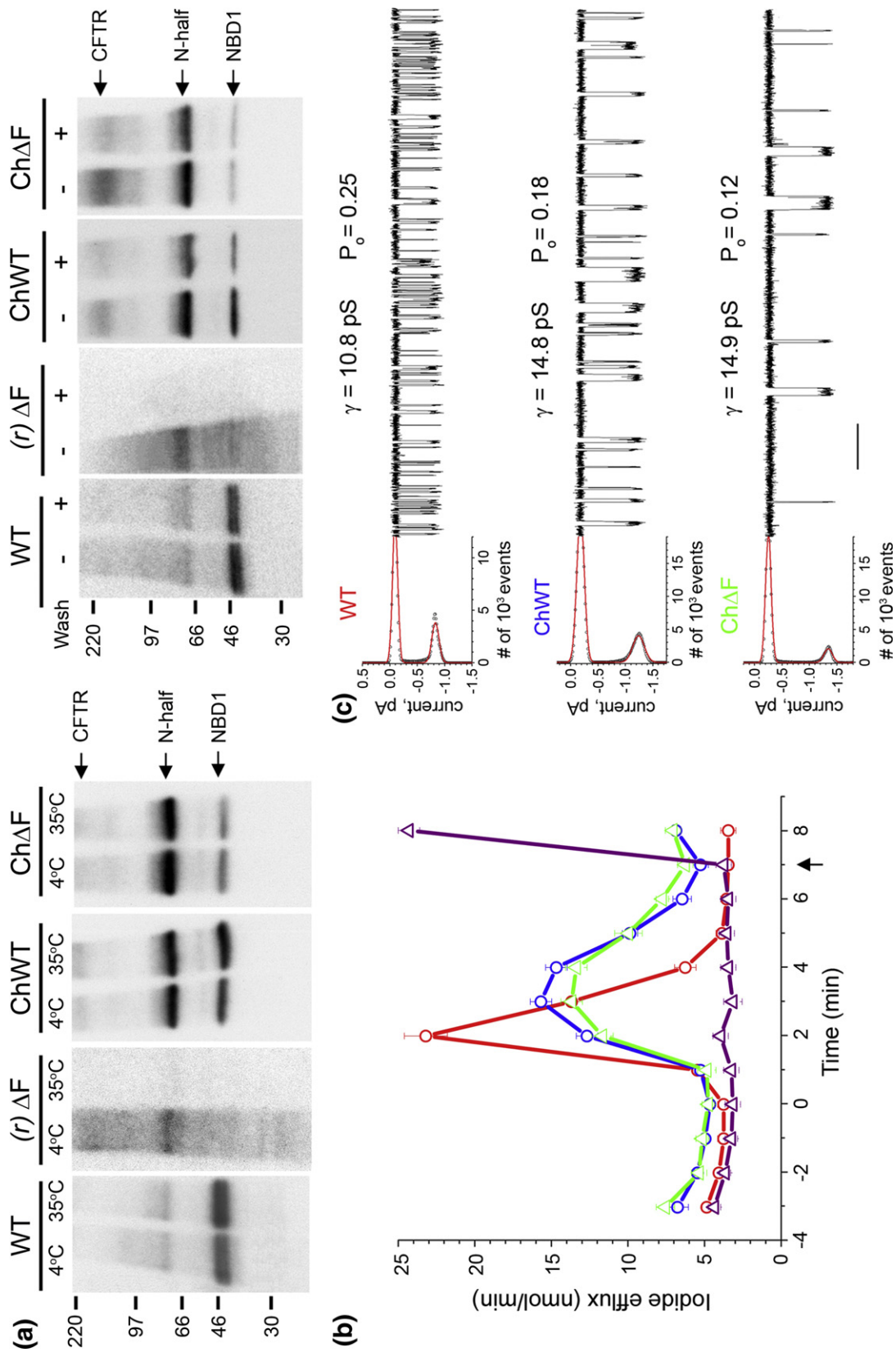
Fig. 3 (*legend on previous page*)

believed to account for a similar level of murine ΔF508 CFTR.[16,21]

However, in general, the other mammalian species were similar to the human, with either a low-level maturation or none at all at the higher temperature. In contrast, there was substantial maturation of the non-mammalian mutants at the higher as well as the lower temperature. With the shark, there was significant maturation at 37 °C but still relatively less than that at 27 °C. With the frog and the chicken proteins, there appeared to be approximately similar amounts of the mature forms present at both temperatures. Thus, the thermal sensitivity of the major cystic-fibrosis-causing mutation appears to be quite different when it is introduced into other species, especially non-mammalian ones.

Biogenesis, lifetime, and function of avian CFTR are relatively insensitive to ΔF509

Although generally highly homologous to human, chicken CFTR has a single amino acid insertion after residue 63 using the human numbering, and thus, in chicken, F509 corresponds to F508 in human. To confirm the apparent ability of chicken ΔF509 CFTR to mature in mammalian cells at mammalian physiological temperature, we performed pulse-chase experiments. Figure 2b shows that conversion of the pulse-labeled immature forms of the WT and mutant chicken proteins to their mature products occurred at similar rates and to similar extents. In fact, the proportion of the pulse-labeled immature form converted to the mature product during a 4-h chase was ~40%, at least as high as or higher than that of the human WT in the same cells under the same conditions.[22] As human ΔF508 CFTR, when stimulated to partially mature in cells at reduced temperature or treated with correcting small molecules, still has a greatly reduced lifetime,[23] we determined if this was also the case with chicken ΔF509 CFTR. Long-term pulse-chase data (Fig. 2c) showed that it was not: the WT and mutant mature proteins decayed at virtually identical rates with a $T_{1/2}$ of ~14 h, remarkably similar to that of human WT protein.[24] Thus, the absence of the F509 residue appeared to have little effect on the biogenesis and lifetime of chicken CFTR.

One important property of CFTR, impaired by ΔF508, is the capacity of NBD1 to tightly bind ATP.[19] Therefore, we tested how the ΔF509 mutation influenced this ability of the chicken protein. In contrast to the human mutant, the chicken mutant retains the ability to bind an ATP analogue at NBD1 at higher (35 °C) as well as lower (4 °C) temperature nearly as effectively as the WT protein (Fig. 3a). Binding to the chicken mutant protein is as thermostable as is its WT counterpart (Fig. 3a, left panel). This tight binding also is reflected in its resistance to being washed off (Fig. 3a, right panel).

Thus, the highly enthalpic ATP binding by NBD1 is retained by the ΔF509 variant of chicken CFTR.

The anion channel activity of ΔF509 chicken CFTR was compared with the WT in iodide efflux experiments and in single-channel recordings. Figure 3b shows similar rates of cAMP-stimulated anion efflux from BHK cells stably expressing either the WT or chicken ΔF509 CFTR. Although the response to stimulation is slightly delayed compared to the WT human, the magnitudes are similar, indicating that the mutant avian channel is functionally competent. A comparison of the single-channel activities at the same temperature (25 °C) with the human WT is shown in Fig. 3c. Most evident is the increased unitary conductance and reduced P_o of both the WT and mutant chicken channels compared to the human. At this temperature, far below the 39 °C to 43 °C body temperature range of chickens, the gating kinetics of the avian channels clearly are slower than that of the human, with the mutant still slower than the WT. Thus, the avian channel responds more slowly to activating stimuli in cells and gates more slowly than the human.

Avian ΔF509 CFTR channel is thermostable

As emphasized in other studies,[19,20] the human ΔF508 channel is characterized by its thermodynamic instability. Having now observed that the chicken ΔF509 channel matures and tightly binds ATP at physiological temperature, we wanted to characterize its single-channel activity over a range of temperatures. As seen in Fig. 4a and b, the gating of the mutant accelerates at increasing temperatures from 30 °C to 40 °C as does that of the WT. This behavior of the chicken WT is quite similar to that of the human WT over this temperature range, but the stability of the chicken mutant is entirely different from that of the human mutant.[14,19] The unitary conductance of the WT and that of mutant chicken channel are the same at each temperature, attesting to the maintenance of the channel integrity even at 40 °C. Intriguingly, the unitary conductance of chicken CFTR in symmetric 300 mM Cl⁻ is not simply 50% higher than that of the human but has a steeper temperature dependence as well, indicating a fundamental difference in ion passage through the open pore structure (Fig. 4c). The open probabilities of the mutant are somewhat lower than those of the WT, but the difference diminishes as the temperature is increased, and notably, the values of even the mutant are higher than those of the WT human at all of these temperatures.

When the conductance and P_o values are expressed as a product, γP_o, which we term the transport capacity of the structural unit, the relative transport abilities of the three channels become very apparent (Fig. 4d). Significantly, at 40 °C, which
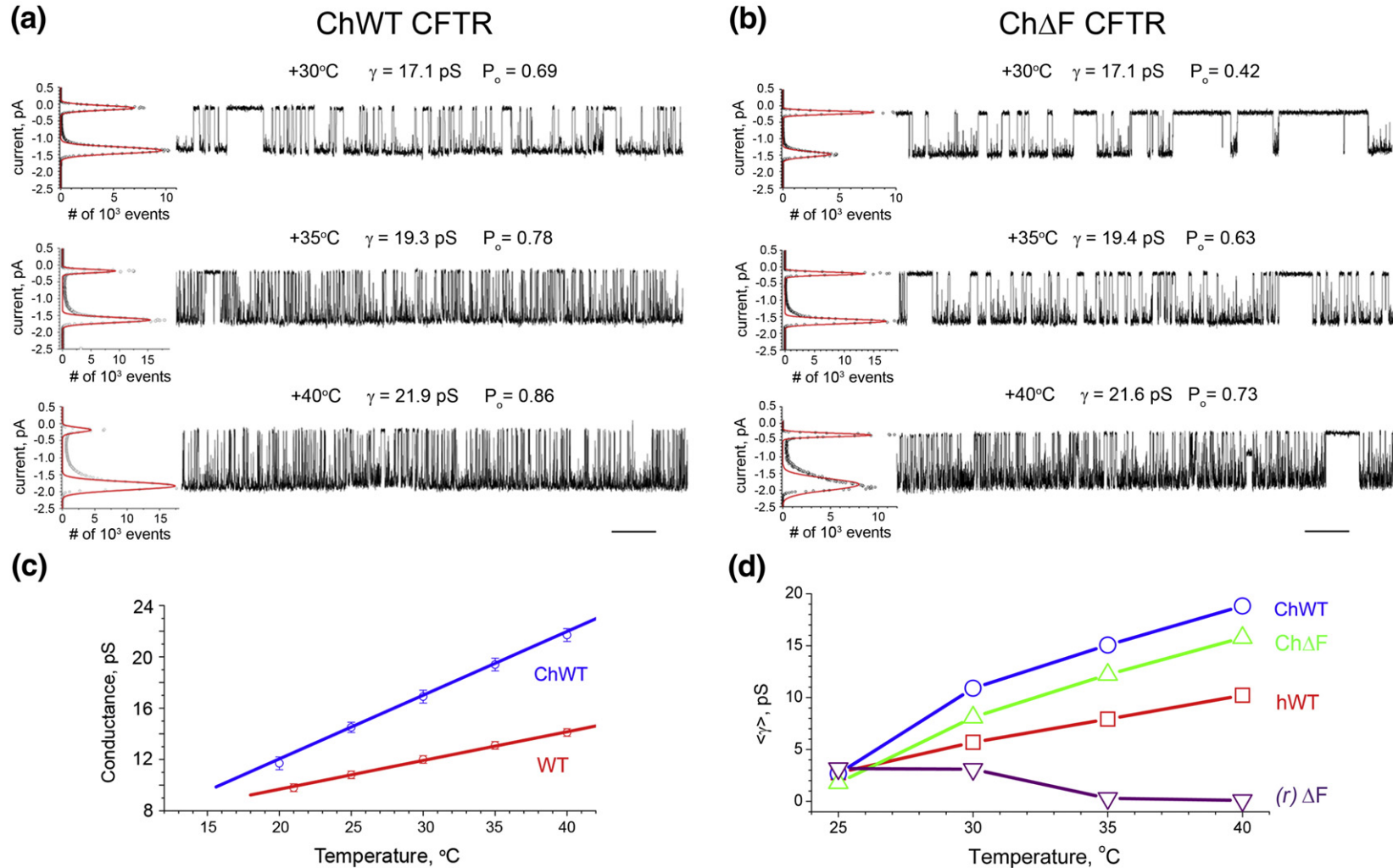
Fig. 4. Avian ΔF509 CFTR channel is nearly as active and thermally stable as the WT. (a) WT chicken CFTR (ChWT) single-channel tracings and all-point histograms fitted by two-peak Gaussians (red line) at the temperatures indicated. The *x*-axis scale bar represents 10 s. (b) ΔF509 chicken CFTR (ChΔF) single-channel current recorded at the same temperatures. The *x*- axis scale bar represents 10 s. (c) Chicken (blue line and symbols) and human (red line and symbols) CFTR single-channel conductance as a function of temperature. Data are shown as mean values ± standard error of the mean. (d) Plots of the transport capacity of the structural unit ⟨γ⟩ for chicken WT (blue) and chicken ΔF509 CFTR (green) at different temperatures compared to human WT (red) and human ΔF508 CFTR (purple). Data are shown as mean value with symbol sizes that exceed the standard error of the mean.

approximates the chicken body temperature, which can range from ~39 °C to 43 °C during a daily cycle, the mutant chicken channel remains highly active. The apparent greater stability and lesser sensitivity to the particular single residue deletion from the avian *versus* the human channel suggest that some key structural or dynamic differences between the proteins must be responsible.

Mimicking chicken CFTR restores thermostability to human ΔF508 CFTR

Although there is a high level of overall sequence conservation among CFTRs in different species, there are non-conservative substitutions at many positions. Concentrating on NBD1 in which changes such as the Teem second site suppressor mutations[25,26] and deletion of the regulatory insertion (RI) sequence[19] are known to stabilize human ΔF508 CFTR, we searched for sequence differences among species that appeared to correlate with the ability of the mutant forms to mature at 37 °C. Among the differences, in addition to the I539T substitution present in many non-human species, we noted a pattern where proline residues replaced other residues in the maturing compared to the non-maturing species (Fig. 5a). In the three non-mammalian species where the ΔF508 mutants mature at 37 °C, prolines replaced other amino acids at several key positions, including at residue A534 in the S539-containing surface loop within the structurally diverse region (SDR) and residue S492 in the Q-loop (Fig. 5b). In the shark sequence, a proline also replaced S495 in the Q-loop. In the chicken sequence, prolines instead of serines were also present at two positions (residues S422 and S434) in the RI. Since chicken CFTR appeared least influenced by the F508 deletion among the species studied, we tested the effect of its four proline substitutions on human ΔF508 CFTR with and without the I539T mutation. As demonstrated by others,[21,25,27] the latter single change enabled some maturation and increase in stability of the human mutant, but in our hands, these were relatively small effects (Fig. 5c), and no normal single-channel gating could be detected at temperatures approaching the mammalian physiological range (see below).

However, the impact of the I539T substitution was much more dramatic when combined with proline replacements at the four positions at which they normally occur in the chicken sequence. Although introduction of all four prolines in the absence of I539T does not promote the maturation of ΔF508 human protein, they have a major effect in its presence, increasing maturation to near the WT level (Fig. 5c). Combination of introduction of a proline into the Q-loop at position 492 together with I539T to generate ΔF/PT was sufficient to allow a high level of maturation even without further addition of the substitutions in the I539 loop (A534P) to generate ΔF/2PT or also in the RI (S422P and S434P) to generate ΔF/4PT. These abbreviations and those of other related constructs studied are precisely defined in the legend to Fig. 5.

Evaluation of the maturation and lifetimes of these variants in pulse-chase experiments confirmed and extended these findings. Figure 5d shows that the immature forms of all these variants decayed at similar rates (upper graph), consistent with earlier studies of WT and mutant human CFTR.[24] However, formation of the mature species was least with I539T alone (ΔF/T) and increased incrementally with inclusion of one, two, and four proline substitutions as judged by the amounts formed by 2 and 4 h (lower graph). Kinetically, in these plots, maturation of the ΔF/T and ΔF/4PT variants appears delayed relative to the other two. However, in the film autoradiograms to the left of the graph, it can be seen that, for ΔF/T (top) and ΔF/4PT (bottom), the density of the immature band impinges strongly on the position of the mature band in the first three lanes, obscuring any differences among them. The relative maximal intensities in the 2- and 4- h lanes are not (or less so) impacted in this way and the differences are clear. The lifetimes of the mature species were assessed in long-term pulse-chase assays (Fig. 5e). With just the I539T (ΔF/T) substitution, a $T_{1/2}$ of ~6 h was observed. With the inclusion of S492P ± A534P (ΔF/PT or ΔF/2PT), the turnover rates were indistinguishable from WT with a $T_{1/2}$ of ~14 h. When prolines also replaced residues 422 and 434 in the RI to form ΔF/4PT, the rate appeared even slower than WT with a $T_{1/2}$ of ~16 h. Thus, the biological stability of the

Fig. 5. Mimicking chicken CFTR (prolines and I539T) restores maturation and lifetime of ΔF508 CFTR. (a) Pattern of proline substitutions in NBD1 of CFTR orthologs with different sensitivities to the ΔF508 mutation. Tabulated are residue positions (human amino acid numbering) where prolines commonly replace other residues in the non-mammalian species in which ΔF508 variants mature at 37 °C and are stable. The common I539T replacement is also indicated. (b) Three-dimensional NBD1 structure (Protein Data Bank ID: 2BBO) is shown with positions of tested residues indicated. RI is colored red, SDR is colored orange, and the F508 loop is colored green. (c) Western blot of WT and ΔF508 CFTR expressed in HEK-293 cells and ΔF508 modified with I539T (ΔF/T), S422P/S434P/S492P/A534P (ΔF/4P), I539T/S492P (ΔF/PT), I539T/S492P/A534P (ΔF/2PT), and I539T/S422P/S434P/S492P/A534P (ΔF/4PT). Methods are as in Fig. 2a. (d) Short-term pulse-chase experiments with variants indicated. Qualitative and quantitative autoradiograms are as in Fig. 2b. Color code: ΔF/T, red; ΔF/PT, orange; ΔF/2PT, green; ΔF/4PT, blue; human WT, black. (e) Long-term pulse-chase experiments performed and analyzed as in Fig. 2c and shown with the same colors as in (b).

Fig. 5 (*legend on previous page*)
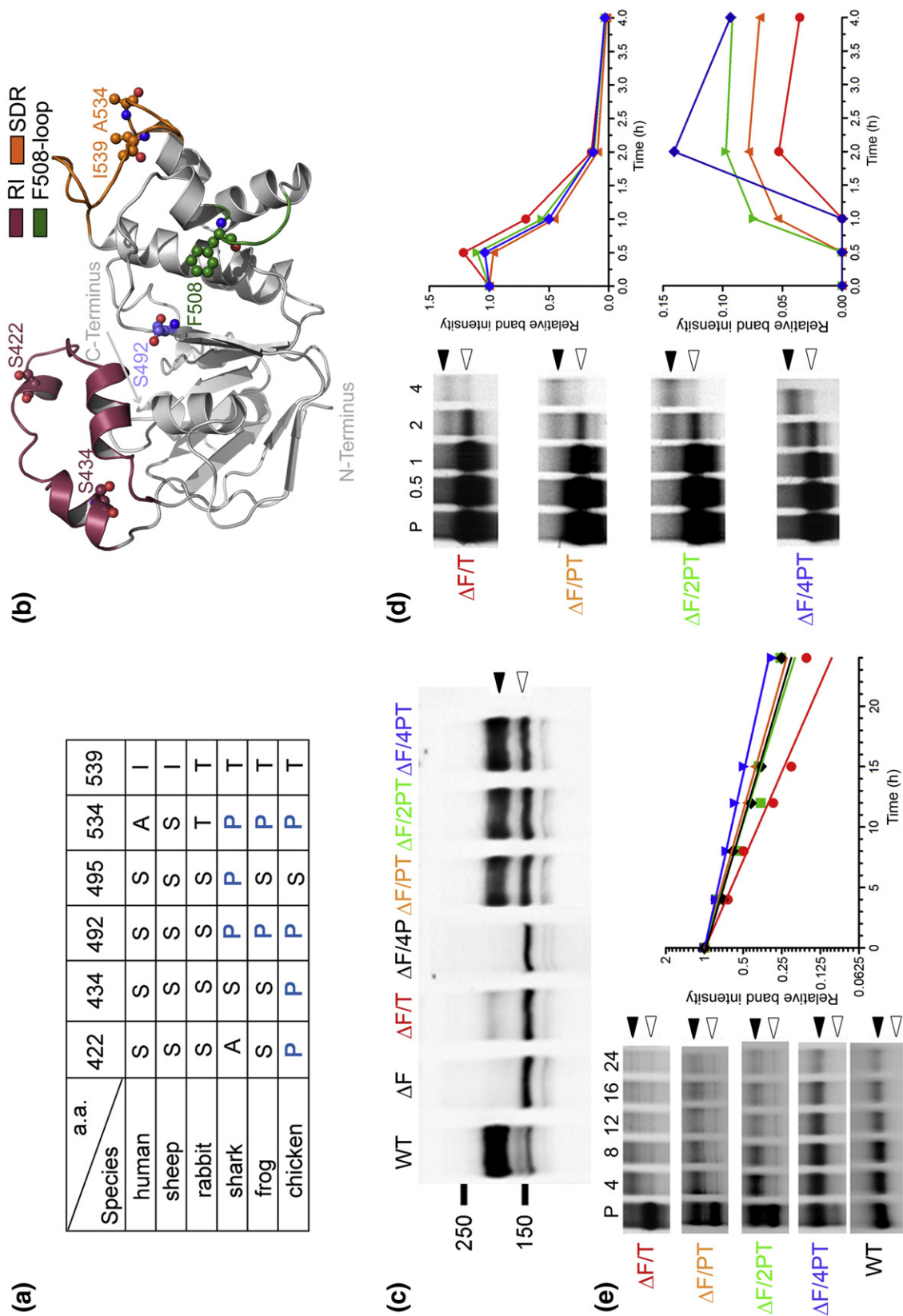
most complete mimic of the chicken protein may exceed that of the human WT.

To determine how these modifications influenced the nucleotide binding function of NBD1 of ΔF508 CFTR, we assessed their effect on the trapping of N_3ATP by NBD1 (Fig. S2). Thermostable binding of the nucleotide by the WT, which is lost in ΔF508 CFTR,[19] was not restored after rescue in cells grown at 27 °C [(*r*)ΔF panel], but was to some extent by I539T (ΔF/T panel), to a greater extent when S492P was added (ΔF/PT panel), still further with A534P also added (ΔF/2PT panel), and to near the WT level with proline replacements at residues S492 and A534 as well (ΔF/4PT panel). Thus, there was greater stable binding at 35 °C and 40 °C with increasing numbers of prolines introduced, reflecting an incremental stabilization towards the WT state.

Proline substitutions restore full-conductance single-channel gating

A similar cumulative stabilizing effect of the proline substitutions was also observed at the single-channel level. At a fixed sub-physiological temperature (35 °C), the I539T/ΔF508 protein exhibited predominantly a fast flickering mode (ffm) with only rare full-conductance channel openings (Fig. 6a). The addition of the S492P substitution generated a dominant full-conductance behavior (ΔF/PT), with a P_o approximately half of the WT human channel at that temperature. Inclusion of a second proline (S534P) reduced this P_o somewhat (ΔF/2PT), while that of the form with four prolines (ΔF/4PT) is further reduced quite substantially (ΔF/4PT), reflecting a markedly slowed gating in this strongly stabilized state.

Stabilizing prolines provide WT-like channel activity at physiological temperature

When temperature was continuously ramped from below to above the physiological range, as indicated in Fig. 6b, the ffm of gating, characteristic of the ΔF508 channel,[19] still dominated the ΔF/T channel over the entire temperature range (upper tracing). Addition of S492P to form ΔF/PT resulted in WT-like full-conductance gating at temperatures up to approximately 37 °C, above which there was a transition to the ffm (middle tracing). Thus, as observed in the 35 °C fixed temperature recording (Fig. 6a), introduction of the Q-loop proline (S492P) had a significant stabilizing effect. However, with continued temperature increase, normal gating was not maintained, but transition to the ffm occurred. In contrast, the inclusion of the additional three prolines to form ΔF/4PT resulted in uniform full-conductance gating, albeit with low frequency at lower temperatures, up to and well above 40 °C (lower tracing). Notably, rather than a continuous

smooth acceleration of gating over the entire temperature range, there is a quite abrupt increase in the frequency of transitions above about 35 °C, reflecting a step change in gating modes.

Thus, an apparent trade-off between thermal stability and level of channel activity was observed, where the most stabilized form with prolines introduced at four positions provided gating similar to the WT at physiological temperature and above, but quite sluggish at lower temperatures. This relationship is very obvious from the temperature dependence of the transport capacity of the structural unit, ⟨γ⟩, which falls off drastically by 35 °C with ΔF/T CFTR. With ΔF/PT, transport increases until that temperature but then decreases precipitously, whereas, with ΔF/4PT, ⟨γ⟩ rises to near-WT levels at 37 °C and 40 °C (Fig. 6c). Thus, both the constant and varying temperature experiments demonstrated a requirement for a balance between thermal stability and channel activity in CFTR, consistent with considerations of such a relationship between stability and catalytic function of proteins in general.[28]

NBD1 stabilization restores an NBD1–CL4 interface

In addition to destabilizing NBD1, deletion of F508 also disrupts interdomain contacts including the interface between the NBD1 surface and the cytoplasmic loop (CL)4 in MSD2 in which the residue normally participates.[29] Specific second-site mutations on either side of this interface (e.g., R1070W or V510D) have been shown to promote maturation of ΔF508 CFTR.[27,30,31] The current observations that the ΔF508 protein with NBD1 strongly stabilized by the proline and I539T substitutions had channel activity similar to the WT at physiological temperature suggested either that the NBD1–CL4 interface is not important for function or that it is adequately restored by NBD1 stabilization. The fact that several cystic-fibrosis-associated missense mutations on the CL4 side of the interface impair either assembly or channel function or both[32] argues against the former alternative and favors the latter. Similarly, the fact that sequences in both the NBD1 and CL4 sides of the interface are identical in human (ΔF sensitive) and chicken (ΔF insensitive) CFTR suggests that the interface is likely to be formed even in the absence of F508 (F509 in the case of chicken). As one test of this possibility, we measured the cross-linking of a pair of cysteine residues across the interface in human ΔF508 CFTR before and after NBD1 stabilization. Using an otherwise Cys-less construct, we had previously observed methanethiosulfonate-mediated cross-linking between V510C and G1069C in WT CFTR.[29,33] Figure 7 shows similar cross-linking of this pair of residues in ΔF/4PT CFTR, providing evidence that the stabilization of ΔF508 NBD1 can
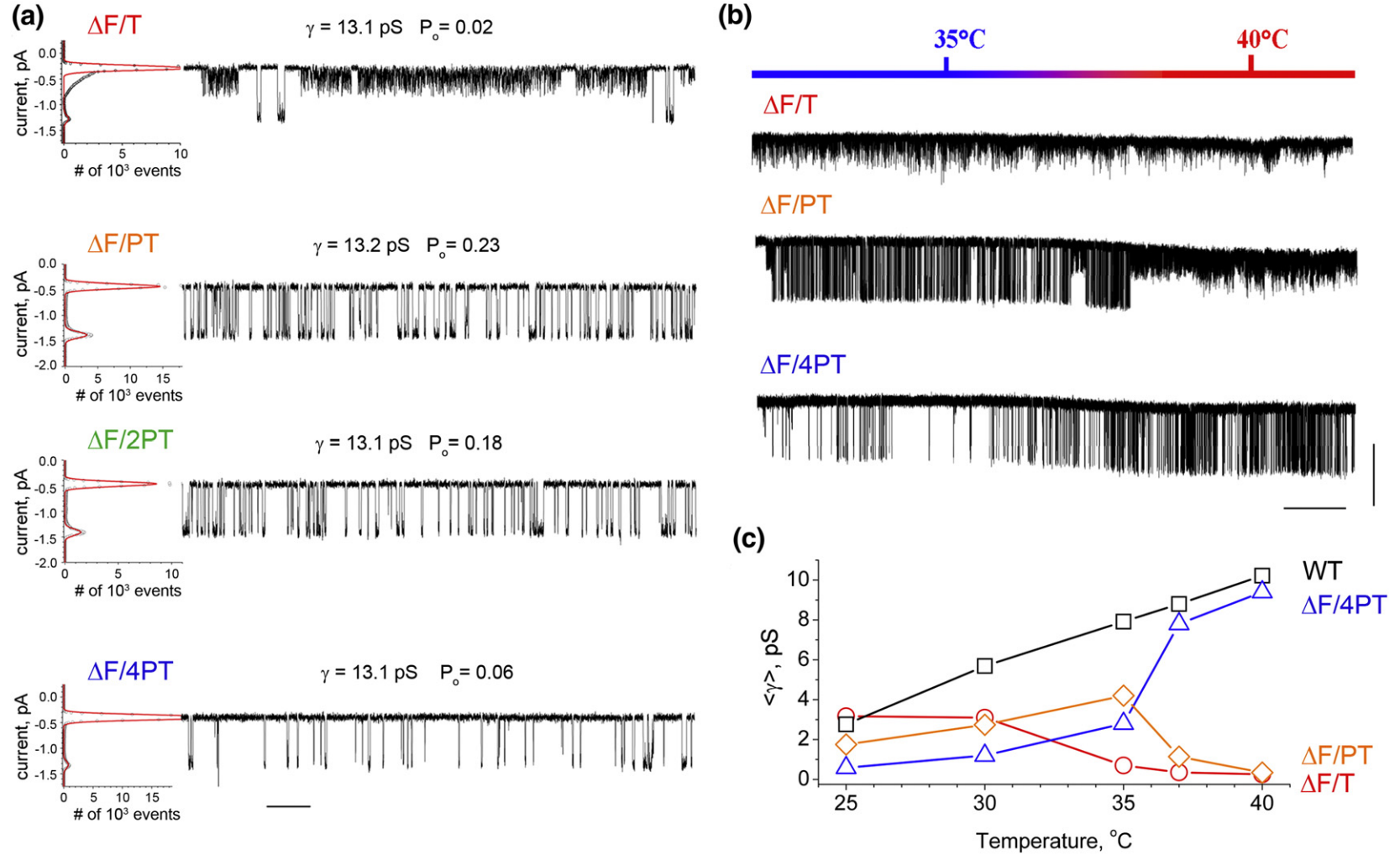
Fig. 6. Proline substitutions reveal trade-off between thermostability and channel activity of ΔF508 CFTR. (a) Single-channel tracings of ΔF508 CFTR with the substitutions indicated. All recordings were prepared at 35 °C. All-point histograms fitted by two-peak Gaussians (red line) are shown on the left of each tracing. The *x*-axis scale bar represents 10 s. (b) Gating of ΔF508 CFTRs with substitutions indicated during a continuous temperature ramp of 1 °C/min. Temperature was maintained at 35 °C for 3 min before initiating the ramp and held at 40 °C for 2 min after this temperature was reached. The *x*- axis scale bar represents 60 s, whereas the *y*-axis scale bar represents 1 pA. (c) Plots of the transport capacity of the structural unit. These ⟨γ⟩ values were calculated after 10 min of incubation at each of the five temperatures indicated to obtain equilibrium values. See Methods for the details of ⟨γ⟩ calculations for the transport unit with unstable open state.

Fig. 7. Restoration of the ΔF508 CFTR NBD1–CL4 interface by proline and I539T mutations. HEK293 cells were transiently transfected with Cys-less CF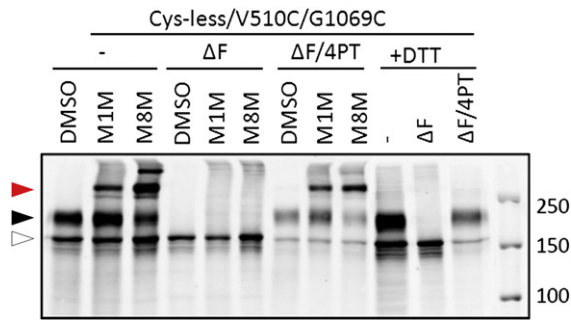TR or Cys-less ΔF508-CFTR in the presence or absence of the 4PT mutations (S422P/S434P/S492P/A534P/I539T), with the Cys pair V510C/G1069C introduced at the CL4/NBD1 interface. Forty-eight hours after transfection, cells were incubated with 200 μM M1M (1,1-methanediyl bis-methane-thiosulfonate) or M8M (1,5-pentanediyl bis-methane-thiosulfonate), and cell lysates in SDS-PAGE sample buffer with or without DTT as indicated were subjected to Western blot analysis with mAb 596. Red arrowhead indicates cross-linked CFTR, filled arrowhead indicates mature complex-glycosylated CFTR, and open arrowhead indicates immature core-glycosylated CFTR.

restore an interaction of the mutant domain with CL4, consistent with the requirement of such an interaction for the high level of maturation and function of the ΔF/4PT protein.

Reversion of avian ΔF509 CFTR to human ΔF508 CFTR-like behavior

To verify the impact of the particular proline and I539 residues targeted, we also made some of the inverse substitutions in chicken ΔF509 CFTR. The single T540I change alone had a dramatic effect, completely preventing maturation at 37 °C (Fig. 8a, lane 2) and allowing only a low level at 27 °C, even

though neither the maturation (not shown) nor the channel function (Fig. 8b, upper tracing) of WT chicken CFTR was influenced by the substitution. This is indicative of the apparently tight linkage between the influences of residues 509 and 540 on maturation. Independent of this very strong influence of T540I on maturation of ΔF509 chicken CFTR, reversion of two of the most stabilizing prolines to the residues at the corresponding positions in human CFTR (P493S and P535A) also severely restricted maturation (Fig. 8a, lane 4). This modest amount of maturation was augmented sufficiently by growth of these cells at 27 °C (Fig. 8a, lane 5) to enable channel function to be assayed. As shown in Fig. 8b (lower tracing), only occasional and short full-conductance openings could be detected at 35 °C with overall transport capacity of the structural unit $\langle \gamma \rangle$ less than 1% of chicken WT. Thus, the absence of the prolines at these two positions strongly destabilizes the ΔF509 chicken CFTR protein, just as their presence stabilizes the human disease-causing mutant.

Proline substitutions improve thermal stability via stabilization of the SDR of ΔF508 NBD1

To gain more insight into the structural basis for stabilization of ΔF508 NBD1 by proline substitutions, we performed molecular dynamics simulations of WT and ΔF508 NBD1 with and without the proline substitutions. We computed the average thermal fluctuations of every residue in the different NBD1 constructs through the course of 15 independent simulations. The profile of thermal fluctuations of WT and ΔF508 NBD1 shows striking differences in two regions—the RI and the SDR—with relatively unaltered values for the rest of the domain (Fig. S3a). Both the RI and the SDR have been hypothesized to influence quaternary assembly of NBD1 with the rest of CFTR.[29,33] Strikingly, substitution of S492 to proline in the context of the I539T mutation
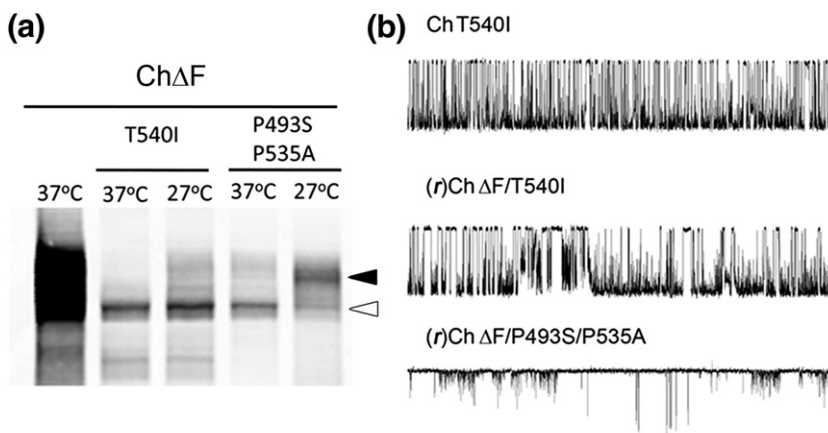
Fig. 8. Avian ΔF509 CFTR is destabilized by reversal of proline and I539T substitutions. (a) Western blot of chicken ΔF509 CFTR showing the influence of the "humanizing" T540I and P493S/P535A substitutions. Cells expressing these variants were grown at the temperatures indicated. (b) Single-channel activity at +35 °C of chicken T540I CFTR substitution (upper tracing); the temperature-rescued chicken ΔF509 CFTR with either the T540I (middle tracing) or the P493S/P535A (lower tracing) substitutions. The x-axis scale bar represents 10 s, whereas the y-axis scale bar represents 1 pA.
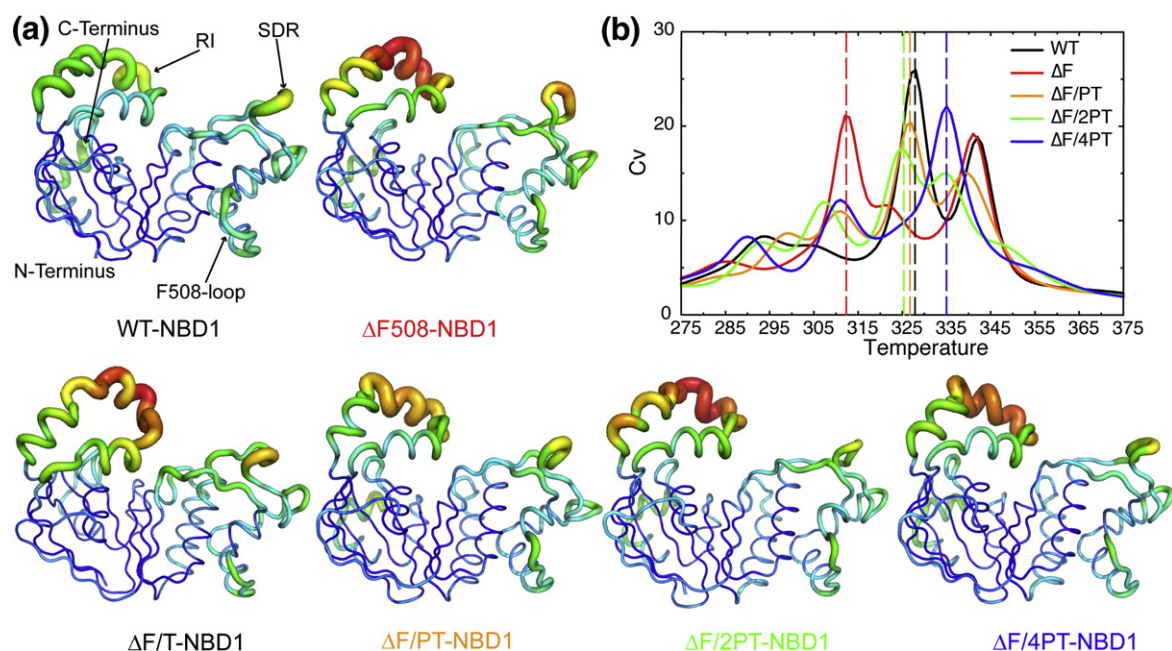
Fig. 9. Stabilization of the SDR with increasing proline substitutions. (a) Tube representation of different NBD1 constructs. The thickness of the tube is proportional to the average root-mean-square fluctuation (RMSF) of the corresponding residue during simulations. Rainbow colors are assigned to residues based on their RMSF values, with blue representing low RMSF and red representing high RMSF. Different regions of NBD1 that influence the dynamics of the domain are marked for WT NBD1. The remaining panels are oriented in the same way as WT NBD1 for simplicity. (b) Cv profile for different NBD1 constructs showing increase in the folding transition temperature with increase in the number of proline substitutions. Peaks in the plot represent structural transitions in NBD1. Broken lines indicate the temperatures—black, ~328 K; red, ~313 K; orange, ~327 K; green, ~326 K; blue, ~335 K—at which major structural transitions take place in the corresponding constructs. See Results and Discussion for further details.

decreased fluctuations in the SDR to values similar to those observed in WT NBD1 (Fig. S3b). Such stabilization of the SDR was not observed in simulations with the I539T substitution alone (Fig. 9a). Thus, addition of proline substitutions decreased fluctuations of the residues comprising not only the loop containing the maturation-reverting substitution site but also that of others in the α-subdomain of NBD1 (Fig. S3b–d). Interestingly, despite the change in fluctuations in the RI, the fluctuations in the SDR and the α-subdomain of NBD1 remain unaltered with increase in the number of proline substitutions (Fig. S3b–d). These results suggest that the dynamics of the RI is uncoupled from that of the other regions with incorporation of proline substitutions.

The proline substitutions do not significantly affect the overall structure of NBD1, as indicated by the profile of the average backbone RMSD from the starting structure (Fig. S4). Mapping of the average thermal fluctuations of every residue as a heat map onto the corresponding structure of NBD1 showed that the regions affected by deletion of F508 are localized to the SDR[34,35] and the F508-containing loop (Fig. 9a). With each additional proline substitution, the SDR region is further stabilized, even beyond WT

NBD1 with four proline substitutions. Thus, while I539T alone did not appear to significantly improve the stability of ΔF508 NBD1, stabilization of the SDR via incorporation of prolines at different positions increased the stability of ΔF508 NBD1.

Molecular dynamics simulations were also performed at different temperatures to help elucidate the thermodynamic basis for stabilization of ΔF508 NBD1 by proline substitutions. The peaks in the specific heat (Cv) plot correspond to tertiary and secondary structural transitions in the protein with increase in temperature. The height of a given peak represents the height of the energy barrier separating the two states. Therefore, the smaller the peak, the easier it is to switch between the corresponding states. The profile of Cv as a function of temperature revealed more than one peak, suggesting multiple structural transitions in the unfolding process (Fig. 9b). Consistent with previously reported thermal unfolding experiments,[7] WT and ΔF508 NBD1 undergo transition towards the unfolded state at ~328 K and ~313 K, respectively (Fig. 9b, black and red broken lines). Comparing the Cv profiles for the different NBD1 constructs, we observed that the folding transition temperature of ΔF508 NBD1 increases with addition of each proline residue

(Fig. 9b). The peaks for different constructs between ∼290 K and ∼300 K correspond to secondary structural rearrangements in NBD1 close to its starting structure (WT, ∼328 K; ΔF, ∼313 K; ΔF/PT, ∼327 K; ΔF/2PT, ∼326 K; ΔF/4PT, ∼335 K) (Fig. 9b, broken lines) (see Discussion). At 342 K, the domain is completely unfolded and the peak corresponds to the formation and collapse of secondary structural elements at high temperatures. Introduction of a proline at S492 in the context of I539T increases the folding transition temperature of ΔF508 NBD1 to ∼327 K, consistent with the observed decrease in thermal fluctuations upon S492P substitution (Fig. 9b, orange broken line). With the addition of each proline substitution, the folding transition temperature increases, even beyond that of WT NBD1 with four proline substitutions (∼335 K) (Fig. 9b, blue broken line).

Discussion

While most attention has been focused on the aberrant biosynthetic processing and trafficking through the secretory pathway of ΔF508 CFTR,[10] the mutant channel had been observed to run down rapidly at physiological temperature,[13] and it more recently has become apparent that the primary impact of the mutation is to decrease the thermodynamic stability of the channel protein.[13,14,19,20] Despite virtually no change from the WT NBD1 fold at the low temperature at which the isolated domain was crystallized,[36] the mutant domain exhibits increased sensitivity to both thermal and chemical denaturation.[7,8] Similarly, the ion channel activity of full-length ΔF508 CFTR is lost at temperatures well below the physiological range.[19] Thus, the major challenge now is to restore a level of stability sufficient to provide near-normal ion channel function and lifetime at the cell surface.

Although the effects of known second site changes (in and proximal to the signature sequence and at I539) have since been studied extensively,[21,27,33,37] their mechanisms of action are still not understood. Additional substitutions, primarily on the surface of NBD1, also empirically discovered to improve solubility during a crystallization project[36] were found to improve the maturation of full-length ΔF508 CFTR in cells.[38] Similarly, deletion of the RI peptide, which enhanced solubility and dimer formation by isolated NBD1,[39] not only greatly improved the maturation and lifetime of the full-length mutant but also restored its thermostability, providing near-normal channel activity at 37 °C and above.[19]

In the current work, we sought a rational approach to discover other allosteric sites in NBD1 where changes might have similar or stronger stabilizing effects. Modulation of protein thermodynamic stability *a priori* remains a general problem in protein chemistry, with approaches generally limited to amino acid substitutions that enhance favorable or remove unfavorable electrostatics or decrease the conformational entropy of the unfolded state.[40] Amino acid substitutions to achieve the latter effect are essentially limited to the introduction of pairs of cysteines to form disulfides or rigid proline residues. The judicious introduction of prolines at multiple sites has been found to increase the thermal stability of many proteins, due to the restriction of the residue by its pyrrolidine ring to fewer conformations than other amino acids.[41]

Earlier work comparing evolutionary conservation of prolines in enzymes from mesophilic and thermophilic organisms detected an increased frequency of the residue at certain sites in the latter.[42] Extensive studies by Matthews *et al.*[43,44] and others[45–47] with a variety of proteins of known three-dimensional structures demonstrated that replacement of residues with prolines could either stabilize or destabilize depending on the sites of their introduction. Clearly, if the residue being replaced contributes to the folded structure, its removal will be destabilizing. The prolines introduced can be more easily accommodated at positions of higher-than-average mobility, where rearrangements that the rigid proline may cause can occur with minimal energetic cost. As a consequence, prolines are generally well accommodated in turns and coils and at the N-termini of α-helices and β-strands.[43] Nevertheless, in practice, despite these guidelines, the selection of residues to be replaced with prolines in a sizeable protein or domain remains largely empirical.

However, when we compared the sequences of CFTR orthologs that remained quite thermostable when the ΔF508 mutation was introduced, the presence of prolines at several sites was apparent (Fig. 5). Each of these locations appeared to satisfy the criteria of stabilizing prolines at mobile unstructured sites, that is, the RI, the Q-loop, and the I539 loop within the SDR (Fig. S5). We recently have shown that the RI has a major influence on ΔF508 CFTR thermal instability.[19] The Q-loop or γ-phosphate switch has variable configurations in different X-ray structures that were observed to influence folding in computational simulations,[48,49] as does the I539 loop. Thus, it is not surprising that a rigidifying effect of prolines in these locations might diminish the thermal instability of ΔF508 NBD1. The apparent additive effects of several substituted prolines acting independently have been observed in other proteins as well.[47]

Molecular dynamics simulations reveal that the SDR of NBD1 is stabilized by the S492P substitution, and the stability further increases with each proline substitution. Clustering of the different configurations assumed by the protein during the simulation at different temperatures revealed that

the smaller peaks in the temperature range of ~280–300 K represent configurations where the RI is flipped out and/or the α-subdomain of NBD1 is partially unfolded (Fig. S6). The first major peak in the Cv profile (Fig. 9b, broken lines) corresponds to the transition from the folded to the unfolded state. A shift in this peak towards lower temperatures represents destabilization, while a shift towards higher temperatures suggests stabilization of the protein. The major peak for ΔF508 NBD1 (at ~313 K) (Fig. 9b, red broken line) shifts significantly to the right with four proline substitutions (to ~335 K) (Fig. 9b, blue broken line). The appearance of an additional peak at ~342 K is a consequence of high entropy of the system at high temperatures. From the simulation trajectories, we observed that the configurations corresponding to the final peak represent transient formation of secondary structural elements that cannot collapse into a folded form due to high temperatures.

A striking feature of the strong stabilizing effect of the proline substitutions was the essentially absolute dependence on the I539T substitution. This dependence contrasts the positive effects on ΔF508 CFTR maturation of other second site changes that are not wholly dependent on I539 T, such as those near the NBD1 signature sequence (G550E/R553M/R555K) and the RI. I539T has an additive effect with the 550/553/555 set.[33] The I539T substitution alone promotes a low level of human ΔF508 CFTR maturation, and its normal presence in murine CFTR probably contributes to the partial maturation of the mouse ΔF508 variant[15,21] as well as that of the rabbit (Fig. 2a). However, this degree of maturation is quite limited compared to the orthologs also containing the proline substitutions described here. The vital role of the hydrophilic threonine residue at the 539 position in determining the fate of ΔF508 CFTR in cells is most clearly demonstrated by the complete prevention of maturation of chicken ΔF509 CFTR by the T540I substitution. Since the residue occupying the 539/540 position has virtually no influence on the WT human or chicken CFTR, there is clearly a tight coupling between the 508 (509) and 539 (540) positions. Having the hydroxyl amino acid at 539 (540) enables a modest level of maturation by an unknown mechanism,[15,21] but this effect is permissive of major stabilization by the key proline substitutions. Their impact is unambiguously confirmed by the fact that their removal completely destabilizes chicken ΔF509 CFTR.

An important finding in this study was the requirement for an appropriate balance between thermostability and CFTR channel function. Thus, as increasing numbers of stabilizing prolines were introduced, channel activity of ΔF508 CFTR diminished at lower temperatures before reaching near-WT open probability and gating rates at physiological temperature. This has important implications for understanding the influence of ΔF508 on channel gating. On the basis of the short-term behavior of the mutant channel on the surface of cells grown at <30 °C, it has generally been described as operating with a P_o approximately 30% of that of the WT.[50] However, as shown in our present and previous[19,20] work, and that of others,[14] this is not the key functional defect that needs to be remedied. Instead, the rapid, essentially complete loss of activity as temperature is raised to the physiological range, as well as the need to restore a level of thermodynamic stability to avoid this loss, is an essential requirement for the development of more effective molecular therapeutic approaches. Significantly, there are now at least three different experimental manipulations that can do this: the combined Teem second site missense mutations,[14] ΔRI,[19] and proline introductions (this study).

All of these manipulations are within NBD1, raising the question of whether stabilizing that domain alone is sufficient to restore maturation and function of the mutant full-length protein. Although the question cannot be definitively answered as yet, the levels of maturation of the chicken ΔF509 CFTR and its human mimic, the lifetime of their mature products, and their channel activities at physiological temperature suggest that repair of NBD1 might be adequate to correct the stability of the full-length mutant protein. With the F508 residue still absent, the important interface of NBD1 with CL4 would remain non-native, and it is known that modification of this interface by substitution of residues on either side, for example, by the V510D[51] and R1070W[27] substitutions, without NBD1 stabilization, improves maturation of ΔF508 CFTR. Nevertheless, the near-WT behavior of ΔF508/4PT suggests that the interface may be slightly rearranged by the stabilized NBD1 such that the connection between domains is adequate for the essential gating–supporting signal transduction across it.[24,25] Biochemical evidence of a restored interface was provided by the cross-linking of cysteine residues placed on either side (Fig. 7). Thus, we have now accumulated strong evidence that thermostabilization of NBD1 has a major restorative influence on full-length ΔF508 CFTR, whereas the so-called rescue of cells in which it is expressed by keeping them at reduced temperature (<30 °C) or exposure of known small-molecule correctors does not. This provides strong motivation for searches for NBD1-stabilizing agents as potential starting points for the development of complementary ΔF508 CFTR corrective therapeutics.

Methods

A mouse monoclonal antibody (mAb 596) recognizing an NBD2 epitope conserved in all species studied was

generated as previously described.[52] Small-molecule correctors VRT-325 and Corrector-4a were generously provided by Cystic Fibrosis Foundation Therapeutics. Recombinant protein kinase A (PKA) catalytic subunit was obtained from Promega. Radiolabeled [γ^{32}P]8N$_3$ATP was obtained from Affinity Labeling Technologies, Inc.; other chemicals were from Sigma. CFTR cDNAs synthesized by GeneArt were kindly provided by Jue Chen (Purdue University).

CFTR expression

CFTR cDNAs encoding WT or mutant proteins were cloned into pcDNA3.1 and pNUT expression vectors for transient expression in HEK-293 cells or stable expression in BHK-21 cells, respectively, as described previously.[19]

Western blotting

HEK-293 or BHK cells overexpressing CFTR were harvested in radioimmunoprecipitation assay (RIPA) buffer without SDS (50 mM Tris, 150 mM NaCl, 1% Triton X-100, and 1% deoxycholate, pH 7.4) plus protease inhibitor cocktail (1 μg/ml leupeptin, 2 μg/ml aprotinin, 3.57 μg/ml E64, 156.6 μg/ml benzamidine, and 2 mM Pefabloc), and equal amounts of protein samples in SDS-PAGE sample buffer were subjected to 7.5% SDS-PAGE and Western blot analysis with mAb 596 to evaluate CFTR expression and maturation.[53]

Metabolic pulse chase

In short-term experiments, BHK cells stably expressing WT or mutant CFTR were grown in 60-mm-diameter dishes and pulsed for 15 min using 1 ml of 100 μCi/ml ^{35}S-methionine (Perkin-Elmer) in methionine-free Dulbecco's modified Eagle's medium. Cells were then washed two times with phosphate-buffered saline (PBS) and chased with growth medium supplemented with 10 mM cold methionine. The chase was stopped by washing two times with cold PBS and solubilizing the cells with RIPA buffer containing the protease inhibitor cocktail. CFTR was immunoprecipitated using mAb 596. The immunoprecipitated proteins were then run on a 7% polyacrylamide gel, fixed with acetic acid–methanol, and soaked in 1 M sodium salicylate for radiography. Band intensity was quantified using a Packard Instant Imager. In long-term experiments, cells were labeled for 8 h in 1.5 ml of methionine-free medium supplemented with 10% normal growth medium, 10% fetal bovine serum, and 66 μCi/ml ^{35}S-methionine and chased using growth medium supplemented with 10 mM unlabeled methionine.

Iodide efflux assay

BHK cells stably expressing WT and mutant CFTR grown to ~100% confluence in six-well plates were incubated in an iodide loading buffer [136 mM NaI, 3 mM KNO$_3$, 2 mM Ca(NO$_3$)$_2$, 11 mM glucose, and 20 mM Hepes, pH 7.4] for 1 h at room temperature. Extracellular iodide was removed by rinsing the cells with iodide-free efflux buffer (same as the loading buffer except NaNO$_3$

replaced NaI). Samples were collected by replacing the efflux buffer (1 ml volume) with fresh solution at 1-min intervals. The first four samples were used to establish the baseline. Iodide efflux upon stimulation with PKA agonists (10 μM forskolin, 100 μM dibutyl-cAMP, and 1 mM 3-isobutyl-1-methylxanthine) was measured using an iodide-selective electrode, LIS-146ICM (Lazar Research Laboratories, Inc.), as previously described.[54] At the end of each assay, efflux buffer containing 0.1% NP-40 was added (arrow) to release retained iodide.

Membrane isolation

BHK or HEK-293 cells expressing CFTR variants were harvested and homogenized on ice in 10 mM Hepes, pH 7.2, and 1 mM ethylenediaminetetraacetic acid containing a protease inhibitor cocktail (benzamidine at 120 μg/ml, E64 at 3.5 μg/ml, aprotinin at 2 μg/ml, leupeptin at 1 μg/ml, and Pefabloc at 50 μg/ml). Centrifugation at 600g for 15 min removed nuclei and undisrupted cells. The supernatant was centrifuged at 100,000g for 60 min to pellet membranes, which were then resuspended in phosphorylation buffer [10 mM Hepes, pH 7.2, containing 0.5 mM ethylene glycol bis(β-aminoethyl ether)N,N'-tetraacetic acid (EGTA), 2 mM MgCl$_2$, and 250 mM sucrose].

Photoaffinity labeling

CFTR nucleotide binding and retention were assayed essentially as previously described.[55] Briefly, membranes containing CFTR were incubated at either 4 °C or 35 °C for 5 min with 25 μM [γ^{32}P]8N$_3$ATP and then UV irradiated directly or after pelleting and washing away unbound nucleotide. To monitor the [γ^{32}P]8N$_3$ATP dissociation from NBD1, we resuspended the washed membranes in nucleotide-free buffer and UV irradiated them after incubation at 35 °C for various periods of time. The labeled membranes were treated with trypsin for 15 min on ice and, after solubilization in RIPA buffer, were immunoprecipitated with immobilized mAbs against NBD1 (L12B4). The immunoprecipitates were resolved by SDS-PAGE (4–20% acrylamide) and transferred to nitrocellulose membranes for autoradiography (X-ray films) and for quantification of ^{32}P radioactivity associated with NBD1-containing bands (Packard Instant Imager, PerkinElmer).

Disulfide cross-linking in whole cells

Disulfide cross-linking of Cys pairs introduced at the NBD1–CL4 interface was carried out as previously described. Briefly, HEK cells transiently expressing Cys-less CFTR constructs with V510C and G1069C substitutions on the WT or ΔF/4PT CFTR basis grown on 35-mm tissue culture dishes were harvested, washed twice in PBS, and resuspended in 60 μl of PBS. Cell suspension (20 μl) was mixed with 40 μl of PBS with dimethyl sulfoxide as vehicle control or PBS containing 300 μM cross-linkers to yield a final concentration of 200 μM of bifunctional cross-linkers from Toronto Research Chemicals: M1M (1,1-methanediyl bismethane-thiosulfonate) and M8M (1,5-

pentanediyl bismethane-thiosulfonate). After a 15-min incubation at room temperature, the cross-linking reaction was stopped with Laemmli sample buffer with or without DTT. Thirty microliters of the samples was loaded on 7.5% SDS-PAGE, and anti-CFTR mAb 596 was used for Western blotting. CFTR was detected with secondary antibodies labeled with infrared dyes (IgG_{2b}-680) using an Odyssey infrared scanner (Licor Inc.).

Patch-clamp single-channel recording

Channel recordings were performed in BHK cells expressing human CFTR using the cell-attached patch-clamp technique implementing an Axopatch 200B amplifier (Axon Instrument/Molecular Device). Prior to recording, cells were perfused with a "cation-free" solution containing 150 mM Tris–HCl, pH 7.2, 1 mM EGTA, and glucose 1 g/L, supplemented with 15 μM forskolin (Sigma-Aldrich). Pipettes (~7–10 MΩ) were filled with 150 mM Tris–HCl, pH 7.2, 1 mM $CaCl_2$, and 3 mM $MgCl_2$. The holding potential was −60 mV. For temperature control, a heating/cooling bath controller (HCC-100A; Dagan Corporation, Minneapolis, MN) was used, equipped with an electronically controlled high-precision (±0.1 °C) and broad-range Peltier thermocouple. Data were filtered with a Bessel low-pass filter (902; Frequency Devices Inc., Haverhill, MA) at a cutoff frequency of 50 Hz and digitized with a sampling rate of 500 Hz using customized Bioquest software. In the cell-attached recordings, the mean conductance of single structural units $\langle\gamma\rangle$ was estimated in continuous recording at each temperature as mean current produced by a particular population of CFTR channels divided by the potential difference between applied potential and potential of zero current ($\Delta V \sim 80$ mV) and the number of channels in the patch. The mean current values were estimated by averaging all non-zero current values that were then corrected by subtraction of mean zero current noise amplitude.

Planar-bilayer-based single-channel recording

Planar lipid bilayers were prepared by painting a 0. 2-mm hole drilled in a Teflon cup with a phospholipid solution in *n*-decane containing a 3:1 mixture of 1-palmitoyl-2-oleoyl-*sn*-glycero-3-phosphoethanolamine and 1-palmitoyl-2-oleoyl-*sn*-glycero-3-phosphoserine (Avanti Polar Lipids). The lipid bilayer separated 1.0 ml of solution (*cis* side) from 5.0 ml of solution (*trans* side). Both chambers were magnetically stirred and thermally insulated. Heating and temperature were controlled with a temperature control system, TC2BIP (Cell Micro Controls).

CFTR ion channels were transferred into the preformed lipid bilayer by spontaneous fusion of membrane vesicles containing CFTR variants. To maintain uniform orientation and functional activity of CFTR channels, we added 2 mM ATP, 50 nM PKA, and membrane vesicles to the *cis* compartment only. All measurements were performed in symmetrical salt solution (300 mM Tris–HCl, pH 7.2, 3 mM $MgCl_2$, and 1 mM EGTA) under voltage-clamp conditions, using an Axopatch 200B amplifier (Axon Instrument/Molecular Device). The membrane voltage

potential of −75 mV is the difference between *cis* and *trans* (ground) compartments. The output signal was filtered with an eight-pole Bessel low-pass filter, LPBF-48DG (NPI Electronic, Tamm, Germany), with a cutoff frequency of 50 Hz, digitized with a sampling rate of 500 Hz and recorded with pClamp 9.2 software. Origin 75 software (Origin Lab Corp., Northampton, MA) was used to fit all-point histograms (pClamp 9.2, Axon Instruments) by multi-peak Gaussians. Single-channel current was defined as the distance between peaks on the fitting curve and used for the calculation of the single-channel conductance. The probability of the single channel being open (P_o) was calculated as a ratio of the area under the peak for the open state to the total area under both peaks on the fitting curve.

The transport capacity of the structural unit was defined as a mean conductance $\langle\gamma\rangle = \gamma P_o$ for WT CFTR and mutants with a single conductive state and stable gating kinetics. Unlike WT CFTR, some mutants, including ∆F508 CFTR, have unstable gating kinetics and variable conductive state, with no well-resolved peaks on the all-point histogram. The transport capacity of the structural unit $\langle\gamma\rangle$ in this case was estimated as a mean current of 10 min of recording divided by the applied potential difference, so as to be an exact analogue of γP_o used for the channels with stable and well-defined open state. The only recordings used were those with openings to a single resolved open state or transiently transformed from unstable gating mode being observed to a gating mode with well-resolved open and closed states. The mean current values were estimated by averaging all non-zero current values that were then corrected by subtraction of mean zero current noise amplitude.

Molecular dynamics simulations

Discrete molecular dynamics (DMD) simulations[56,57] were performed using NBD1 coordinates (Protein Data Bank ID: 2BBO). Solubilizing mutations were reverted back to their native amino acids using Medusa[58] to obtain the starting structure for simulations. The amino acids in the RI were modeled *ab initio* using DMD simulations. Energy minimization of the generated structural model was performed using Chiron.[59] Using the minimized structural model of WT NBD1, we performed 15 independent simulations, each spanning 10^5 DMD time units, after assigning to the atoms initial velocities that are generated using a random seed each time. The relation between DMD time units and real time was described previously.[60] Covariation analysis was performed on the simulation trajectories, and root-mean-square fluctuation of every amino acid was computed as previously described.[60]

The weighted histogram analysis method (WHAM)[61] was used to compute the specific heat (Cv) of different NBD1 constructs. The program used to perform WHAM calculations was obtained from the MMTSB toolkit.[62] Briefly, WHAM utilizes multiple simulation trajectories with overlapping sampling along the chosen reaction coordinates to compute the density of states. Using the density of states, one can compute the Cv of the protein at different temperatures according to the partition function $Z = \int\rho(E)\exp\{-E/kT\}\mathrm{d}E$, where $\rho(E)$ represents the density of states, E represents energy, k is the Boltzmann constant, and T represents temperature. More details of the method

are described elsewhere.[61] Simulations were performed for 10^6 DMD time units at temperatures starting from 0.55 DMD units (~275 K) to 0.75 DMD units (~375 K) at increments of 0.01 DMD units (~5 K). Trajectories from simulations performed at all temperatures were used to compute Cv. Taking the time required for relaxation of the system into account, the first 10^5 time units were excluded, and the remaining 9×10^5 time units were used.

Statistics

Data are expressed as mean ± standard error of the mean; p values were calculated using unpaired Student's t test. A p value < 0.05 was considered significant.

Supplementary Data

Supplementary data associated with this article can be found, in the online version, at doi:10.1016/j.jmb.2012.03.001

References

1. Cheng, S. H., Gregory, R. J., Marshall, J., Paul, S., Souza, D. W., White, G. A. *et al.* (1990). Defective intracellular transport and processing of CFTR is the molecular basis of most cystic fibrosis. *Cell*, **63**, 827–834.
2. Riordan, J. R. (2005). Assembly of functional CFTR chloride channels. *Annu. Rev. Physiol.* **67**, 701–718.
3. Denning, G. M., Anderson, M. P., Amara, J. F., Marshall, J., Smith, A. E. & Welsh, M. J. (1992). Processing of mutant cystic fibrosis transmembrane conductance regulator is temperature-sensitive. *Nature*, **358**, 761–764.
4. Kopito, R. R. (1999). Biosynthesis and degradation of CFTR. *Physiol. Rev.* **79**, S167–173.
5. Zhang, F., Kartner, N. & Lukacs, G. L. (1998). Limited proteolysis as a probe for arrested conformational maturation of delta F508 CFTR. *Nat. Struct. Biol.* **5**, 180–183.
6. Qu, B. H., Strickland, E. H. & Thomas, P. J. (1997). Localization and suppression of a kinetic defect in cystic fibrosis transmembrane conductance regulator folding. *J. Biol. Chem.* **272**, 15739–15744.
7. Protasevich, I., Yang, Z., Wang, C., Atwell, S., Zhao, X., Emtage, S. *et al.* (2010). Thermal unfolding studies show the disease causing F508del mutation in CFTR thermodynamically destabilizes nucleotide-binding domain 1. *Protein Sci.* **19**, 1917–1931.
8. Wang, C., Protasevich, I., Yang, Z., Seehausen, D., Skalak, T., Zhao, X. *et al.* (2010). Integrated biophysical studies implicate partial unfolding of NBD1 of CFTR in the molecular pathogenesis of F508del cystic fibrosis. *Protein Sci.* **19**, 1932–1947.
9. Lewis, H. A., Zhao, X., Wang, C., Sauder, J. M., Rooney, I., Noland, B. W. *et al.* (2005). Impact of the deltaF508 mutation in first nucleotide-binding domain of human cystic fibrosis transmembrane conductance regulator on domain folding and structure. *J. Biol. Chem.* **280**, 1346–1353.
10. Lukacs, G. L. & Verkman, A. S. (2011). Insights into CFTR folding, misfolding and correction of the deltaF508 CFTR conformational defect. *Trends Mol. Med.* **18**, 81–91.
11. Van Goor, F., Hadida, S., Grootenhuis, P. D., Burton, B., Stack, J. H., Straley, K. S. *et al.* (2011). Correction of the F508del-CFTR protein processing defect in vitro by the investigational drug VX-809. *Proc. Natl Acad. Sci. USA*, **108**, 18843–18848.
12. Pedemonte, N., Lukacs, G. L., Du, K., Caci, E., Zegarra-Moran, O., Galietta, L. J. & Verkman, A. S. (2005). Small-molecule correctors of defective DeltaF508-CFTR cellular processing identified by high-throughput screening. *J. Clin. Invest.* **115**, 2564–2571.
13. Schultz, B. D., Frizzell, R. A. & Bridges, R. J. (1999). Rescue of dysfunctional Delta F508-CFTR chloride channel activity by IBMX. *J. Membr. Biol.* **170**, 51–66.
14. Wang, W., Okeyo, G. O., Tao, B., Hong, J. S. & Kirk, K. L. (2011). Thermally unstable gating of the most common cystic fibrosis mutant channel ({Delta}F508): 'Rescue' by suppressor mutations in nucleotide binding domain 1 and by constitutive mutations in the cytosolic loops. *J. Biol. Chem.* **286**, 41937–41948.
15. Ostedgaard, L. S., Rogers, C. S., Dong, Q. A., Randak, C. O., Vermeer, D. W., Rokhlina, T. *et al.* (2007). Processing and function of CFTR-Delta F508 are species-dependent. *Proc. Natl Acad. Sci. USA*, **104**, 15370–15375.
16. Dong, Q., Ostedgaard, L. S., Rogers, C., Vermeer, D. W., Zhang, Y. P. & Welsh, M. J. (2012). Human-mouse cystic fibrosis transmembrane conductance regulator (CFTR) chimeras identify regions that partially rescue CFTR-Delta F508 processing and alter its gating defect. *Proc. Natl Acad. Sci. USA*, **109**, 917–922.
17. Price, M. P., Ishihara, H., Sheppard, D. N. & Welsh, M. J. (1996). Function of *Xenopus* cystic fibrosis transmembrane conductance regulator (CFTR) Cl⁻ channels and use of human-*Xenopus* chimeras to investigate the pore properties of CFTR. *J. Biol. Chem.* **271**, 25184–25191.
18. Hanrahan, J. W., Duguay, F., Sansom, S., Alon, N., Jensen, T. J., Riordan, J. R. & Grzelczak, Z. (1993). Low-conductance chloride channel activated by cAMP in the rectal gland of the shark *Squalus acanthias* and in cells heterologously expressing the shark CFTR gene. *MDIBL Bull.* **32**, 48–49.
19. Aleksandrov, A. A., Kota, P., Aleksandrov, L. A., He, L., Jensen, T., Cui, L. *et al.* (2010). Regulatory insertion removal restores maturation, stability and function of DeltaF508 CFTR. *J. Mol. Biol.* **401**, 194–210.
20. Hegedus, T., Aleksandrov, A., Cui, L., Gentzsch, M., Chang, X. B. & Riordan, J. R. (2006). F508del CFTR with two altered RXR motifs escapes from ER quality

control but its channel activity is thermally sensitive. *Biochim. Biophys. Acta*, **1758**, 565–572.

21. Hoelen, H., Kleizen, B., Schmidt, A., Richardson, J., Charitou, P., Thomas, P. J. & Braakman, I. (2010). The primary folding defect and rescue of DeltaF508 CFTR emerge during translation of the mutant domain. *PLoS One*, **5**, e15458.

22. Du, K., Sharma, M. & Lukacs, G. L. (2005). The DeltaF508 cystic fibrosis mutation impairs domain–domain interactions and arrests post-translational folding of CFTR. *Nat. Struct. Mol. Biol.* **12**, 17–25.

23. Okiyoneda, T., Barriere, H., Bagdany, M., Rabeh, W. M., Du, K., Hohfeld, J. *et al.* (2010). Peripheral protein quality control removes unfolded CFTR from the plasma membrane. *Science*, **329**, 805–810.

24. Ward, C. L. & Kopito, R. R. (1994). Intracellular turnover of cystic fibrosis transmembrane conductance regulator. Inefficient processing and rapid degradation of wild-type and mutant proteins. *J. Biol. Chem.* **269**, 25710–25718.

25. DeCarvalho, A. C., Gansheroff, L. J. & Teem, J. L. (2002). Mutations in the nucleotide binding domain 1 signature motif region rescue processing and functional defects of cystic fibrosis transmembrane conductance regulator delta f508. *J. Biol. Chem.* **277**, 35896–35905.

26. Teem, J. L., Berger, H. A., Ostedgaard, L. S., Rich, D. P., Tsui, L. C. & Welsh, M. J. (1993). Identification of revertants for the cystic fibrosis delta F508 mutation using STE6-CFTR chimeras in yeast. *Cell*, **73**, 335–346.

27. Thibodeau, P. H., Richardson, J. M., III, Wang, W., Millen, L., Watson, J., Mendoza, J. L. *et al.* (2010). The cystic fibrosis-causing mutation deltaF508 affects multiple steps in cystic fibrosis transmembrane conductance regulator biogenesis. *J. Biol. Chem.* **285**, 35825–35835.

28. Whitford, P. C., Onuchic, J. N. & Wolynes, P. G. (2008). Energy landscape along an enzymatic reaction trajectory: hinges or cracks? *HFSP J.* **2**, 61–64.

29. Serohijos, A. W., Hegedus, T., Aleksandrov, A. A., He, L., Cui, L., Dokholyan, N. V. & Riordan, J. R. (2008). Phenylalanine-508 mediates a cytoplasmic-membrane domain contact in the CFTR 3D structure crucial to assembly and channel function. *Proc. Natl Acad. Sci. USA*, **105**, 3256–3261.

30. Wang, Y., Loo, T. W., Bartlett, M. C. & Clarke, D. M. (2007). Correctors promote maturation of cystic fibrosis transmembrane conductance regulator (CFTR)-processing mutants by binding to the protein. *J. Biol. Chem.* **282**, 33247–33251.

31. Loo, T. W., Bartlett, M. C. & Clarke, D. M. (2010). The V510D suppressor mutation stabilizes DeltaF508-CFTR at the cell surface. *Biochemistry*, **49**, 6352–6357.

32. Seibert, F. S., Linsdell, P., Loo, T. W., Hanrahan, J. W., Clarke, D. M. & Riordan, J. R. (1996). Disease-associated mutations in the fourth cytoplasmic loop of cystic fibrosis transmembrane conductance regulator compromise biosynthetic processing and chloride channel activity. *J. Biol. Chem.* **271**, 15139–15145.

33. He, L., Aleksandrov, A. A., Serohijos, A. W., Hegedus, T., Aleksandrov, L. A., Cui, L. *et al.* (2008). Multiple membrane-cytoplasmic domain contacts in the cystic fibrosis transmembrane conductance regulator (CFTR) mediate regulation of channel gating. *J. Biol. Chem.* **283**, 26383–26390.

34. Zaitseva, J., Oswald, C., Jumpertz, T., Jenewein, S., Wiedenmann, A., Holland, I. B. & Schmitt, L. (2006). A structural analysis of asymmetry required for catalytic activity of an ABC-ATPase domain dimer. *EMBO J.* **25**, 3432–3443.

35. Lewis, H. A., Wang, C., Zhao, X., Hamuro, Y., Conners, K., Kearins, M. C. *et al.* (2010). Structure and dynamics of NBD1 from CFTR characterized using crystallography and hydrogen/deuterium exchange mass spectrometry. *J. Mol. Biol.* **396**, 406–430.

36. Lewis, H. A., Buchanan, S. G., Burley, S. K., Conners, K., Dickey, M., Dorwart, M. *et al.* (2004). Structure of nucleotide-binding domain 1 of the cystic fibrosis transmembrane conductance regulator. *EMBO J.* **23**, 282–293.

37. Roxo-Rosa, M., Xu, Z., Schmidt, A., Neto, M., Cai, Z. W., Soares, C. M. *et al.* (2006). Revertant mutants G550E and 4RK rescue cystic fibrosis mutants in the first nucleotide-binding domain of CFTR by different mechanisms. *Proc. Natl Acad. Sci. USA*, **103**, 17891–17896.

38. Pissarra, L. S., Farinha, C. M., Xu, Z., Schmidt, A., Thibodeau, P. H., Cai, Z. *et al.* (2008). Solubilizing mutations used to crystallize one CFTR domain attenuate the trafficking and channel defects caused by the major cystic fibrosis mutation. *Chem. Biol.* **15**, 62–69.

39. Atwell, S., Brouillette, C. G., Conners, K., Emtage, S., Gheyi, T., Guggino, W. B. *et al.* (2010). Structures of a minimal human CFTR first nucleotide-binding domain as a monomer, head-to-tail homodimer, and pathogenic mutant. *Protein Eng. Des. Sel.* **23**, 375–384.

40. Kumar, S., Tsai, C. J. & Nussinov, R. (2000). Factors enhancing protein thermostability. *Protein Eng.* **13**, 179–191.

41. Prajapati, R. S., Das, M., Sreeramulu, S., Sirajuddin, M., Srinivasan, S., Krishnamurthy, V. *et al.* (2007). Thermodynamic effects of proline introduction on protein stability. *Proteins*, **66**, 480–491.

42. Watanabe, K., Chishiro, K., Kitamura, K. & Suzuki, Y. (1991). Proline residues responsible for thermostability occur with high frequency in the loop regions of an extremely thermostable oligo-1,6-glucosidase from *Bacillus thermoglucosidasius* KP1006. *J. Biol. Chem.* **266**, 24287–24294.

43. Matthews, B. W., Nicholson, H. & Becktel, W. J. (1987). Enhanced protein thermostability from site-directed mutations that decrease the entropy of unfolding. *Proc. Natl Acad. Sci. USA*, **84**, 6663–6667.

44. Nicholson, H., Tronrud, D. E., Becktel, W. J. & Matthews, B. W. (1992). Analysis of the effectiveness of proline substitutions and glycine replacements in increasing the stability of phage T4 lysozyme. *Biopolymers*, **32**, 1431–1441.

45. Bogin, O., Peretz, M., Hacham, Y., Korkhin, Y., Frolow, F., Kalb, A. J. & Burstein, Y. (1998). Enhanced thermal stability of *Clostridium beijerinckii* alcohol dehydrogenase after strategic substitution of amino acid residues with prolines from the homologous thermophilic *Thermoanaerobacter brockii* alcohol dehydrogenase. *Protein Sci.* **7**, 1156–1163.

46. Ge, M. & Pan, X. M. (2009). The contribution of proline residues to protein stability is associated with isomerization equilibrium in both unfolded and folded states. *Extremophiles*, **13**, 481–489.

47. Takano, K., Higashi, R., Okada, J., Mukaiyama, A., Tadokoro, T., Koga, Y. & Kanaya, S. (2009). Proline effect on the thermostability and slow unfolding of a hyperthermophilic protein. *J. Biochem.* **145**, 79–85.

48. Bisignano, P. & Moran, O. (2010). Molecular dynamics analysis of the wild type and dF508 mutant structures of the human CFTR-nucleotide binding domain 1. *Biochimie*, **92**, 51–57.

49. Wieczorek, G. & Zielenkiewicz, P. (2008). DeltaF508 mutation increases conformational flexibility of CFTR protein. *J. Cyst. Fibros.* **7**, 295–300.

50. Dalemans, W., Barbry, P., Champigny, G., Jallat, S., Dott, K., Dreyer, D. *et al.* (1991). Altered chloride-ion channel kinetics associated with the Delta-F508 cystic-fibrosis mutation. *Nature*, **354**, 526–528.

51. Loo, T. W., Bartlett, M. C. & Clarke, D. M. (2011). Benzbromarone stabilizes DeltaF508 CFTR at the cell surface. *Biochemistry*, **50**, 4393–4395.

52. Cui, L., Aleksandrov, L., Chang, X. B., Hou, Y. X., He, L., Hegedus, T. *et al.* (2007). Domain interdependence in the biosynthetic assembly of CFTR. *J. Mol. Biol.* **365**, 981–994.

53. Cui, L., Aleksandrov, L., Hou, Y. X., Gentzsch, M., Chen, J. H., Riordan, J. R. & Aleksandrov, A. A. (2006). The role of cystic fibrosis transmembrane conductance regulator phenylalanine 508 side chain in ion channel gating. *J. Physiol.* **572**, 347–358.

54. Chang, X. B., Tabcharani, J. A., Hou, Y. X., Jensen, T. J., Kartner, N., Alon, N. *et al.* (1993). Protein kinase A (PKA) still activates CFTR chloride channel after mutagenesis of all 10 PKA consensus phosphorylation sites. *J. Biol. Chem.* **268**, 11304–11311.

55. Aleksandrov, L., Mengos, A., Chang, X., Aleksandrov, A. & Riordan, J. R. (2001). Differential interactions of nucleotides at the two nucleotide binding domains of the cystic fibrosis transmembrane conductance regulator. *J. Biol. Chem.* **276**, 12918–12923.

56. Dokholyan, N. V., Buldyrev, S. V., Stanley, H. E. & Shakhnovich, E. I. (1998). Discrete molecular dynamics studies of the folding of a protein-like model. *Folding Des.* **3**, 577–587.

57. Ding, F., Tsao, D., Nie, H. & Dokholyan, N. V. (2008). Ab initio folding of proteins with all-atom discrete molecular dynamics. *Structure*, **16**, 1010–1018.

58. Ding, F. & Dokholyan, N. V. (2006). Emergence of protein fold families through rational design. *PLoS Comput. Biol.* **2**, e85.

59. Ramachandran, S., Kota, P., Ding, F. & Dokholyan, N. V. (2011). Automated minimization of steric clashes in protein structures. *Proteins*, **79**, 261–270.

60. Sharma, S., Ding, F. & Dokholyan, N. V. (2007). Multiscale modeling of nucleosome dynamics. *Biophys. J.* **92**, 1457–1470.

61. Kumar, S., Bouzida, D., Swendsen, R. H., Kollman, P. A. & Rosenberg, J. M. (1992). The weighted histogram analysis method for free-energy calculations on biomolecules. I. The method. *J. Comput. Chem.* **13**, 1011–1021.

62. Feig, M., Karanicolas, J. & Brooks, C. L., III (2004). MMTSB Tool Set: enhanced sampling and multiscale modeling methods for applications in structural biology. *J. Mol. Graphics Modell.* **22**, 377–395.